The Journal of Experimental Biology 200, 767–784 (1997)
Printed in Great Britain © The Company of Biologists Limited 1997
JEB0578

ANGUILLIFORM LOCOMOTION IN AN ELONGATE SALAMANDER (*SIREN INTERMEDIA*): EFFECTS OF SPEED ON AXIAL UNDULATORY MOVEMENTS

GARY B. GILLIS*

Department of Ecology and Evolutionary Biology, University of California, Irvine, CA 92717, USA

Accepted 25 November 1996

Summary

Many workers interested in the mechanics and kinematics of undulatory aquatic locomotion have examined swimming in fishes that use a carangiform or subcarangiform mode. Few empirical data exist describing and quantifying the movements of elongate animals using an anguilliform mode of swimming. Using high-speed video, I examine the axial undulatory kinematics of an elongate salamander, *Siren intermedia*, in order to provide data on how patterns of movement during swimming vary with body position and swimming speed. In addition, swimming kinematics are compared with those of other elongate vertebrates to assess the similarity of undulatory movements within the anguilliform locomotor mode. In *Siren*, most kinematic patterns vary with longitudinal position. Tailbeat period and frequency, stride length, Froude efficiency and the lateral velocity and angle of attack of tail segments all vary significantly with swimming speed. Although swimming speed does not show a statistically significant effect on kinematic variables such as maximum undulatory amplitude (which increases non-linearly along the body), intervertebral flexion and path angle, examination of the data suggests that speed probably has subtle and site-specific effects on these variables which are not detected here owing to the small sample size. Maximum lateral displacement and flexion do not coincide in time within a given tailbeat cycle. Furthermore, the maximum orientation (angle with respect to the animal's direction of forward movement) and lateral velocity of tail segments also do not coincide in time. Comparison of undulatory movements among diverse anguilliform swimmers suggests substantial variation across taxa in parameters such as tailbeat amplitude and in the relationship between tailbeat frequency and swimming speed. This variation is probably due, in part, to external morphological differences in the shape of the trunk and tail among these taxa.

Key words: locomotion, swimming, kinematics, behavior, salamander, *Siren intermedia*.

Introduction

The physical basis underlying all types of locomotion derives from Newton's third law of mechanics, that of action and reaction. To move, an animal must push against the surroundings in its environment (the action). These surroundings will provide resistance and 'push' back (the reaction), propelling the animal through the environment (Gray, 1933). Aquatic vertebrates use a variety of methods to push against and move through their surroundings. In general, these methods can be divided into those in which oscillatory movements (typically of paired appendages) are utilized and those in which undulatory movements (of the axial skeleton or appendages) are used (Webb and Blake, 1985).

In his classic review of fish locomotion, Breder (1926) classified axial-based undulatory locomotor modes into three broad categories: ostraciiform, carangiform and anguilliform. At one extreme of the axial undulatory spectrum (ostraciiform mode), the animal's body is quite rigid and movements of the tail are used to generate propulsive thrust. In contrast, in the anguilliform mode the animal's body is elongate and flexible and during swimming undulatory movements of most, if not all, of the body are used for propulsion.

While a large body of detailed empirical work exists describing the mechanics and kinematics of undulatory aquatic locomotion in vertebrates, much of it pertains to fishes, and most previous work has focused on the more intermediate carangiform and subcarangiform modes of the undulatory spectrum (e.g. Archer and Johnston, 1989; Bainbridge, 1958, 1963; Jayne and Lauder, 1995; Long *et al.* 1994; Videler, 1981; Videler and Hess, 1984; Webb *et al.* 1984). In contrast, much less work has been performed on the more extreme undulatory modes of Breder's spectrum, including that used by elongate vertebrates, anguilliform locomotion.

Elongation of the body has evolved independently in many groups of fishes, and a number of tetrapod lineages as well (Gans, 1975), and most elongate vertebrate swimmers have converged upon an anguilliform mode of locomotion. Among the diverse taxa that utilize this locomotor mode, dramatic morphological variation in axial musculoskeletal structures is

*e-mail: gbgillis@uci.edu.

present (Auffenberg, 1962). In addition to broad variation in axial muscle morphology and the number of vertebrae across taxa, there are also differences in the size and shape of the bodies and tails of elongate fishes, salamanders and reptiles. Yet, despite this phylogenetic diversity, much of what we know about anguilliform swimming comes from only a few analyses of swimming anguillid eels (Gray, 1933; Grillner and Kashin, 1976) and snakes (Jayne, 1985; Graham *et al.* 1987). And, although anguilliform swimmers are believed to use movements of nearly their entire body during locomotion, previous analyses have often not described in detail the precise pattern of longitudinal variation in axial movements. Hence, quantitative analyses of movements of the entire body should reveal the nature of longitudinal variation (within an individual) in kinematic patterns. In addition, comparative kinematic data from distantly related taxa would provide an opportunity to understand better the extent to which phylogenetic differences in locomotor morphology might affect locomotor movements.

In the present study, I examine the structure and movements of the axial skeleton of an elongate salamander, *Siren intermedia*, during swimming at a variety of speeds. My goals are (1) to describe the pattern of segmentation of the axial skeleton of sirenid salamanders, (2) to describe axial movements along the entire body during undulatory locomotion and investigate the extent to which these movements change with speed, and (3) to compare the kinematic patterns of *Siren intermedia* with those of other anguilliform taxa to determine whether phylogenetic differences are related to clear distinctions in locomotor movements.

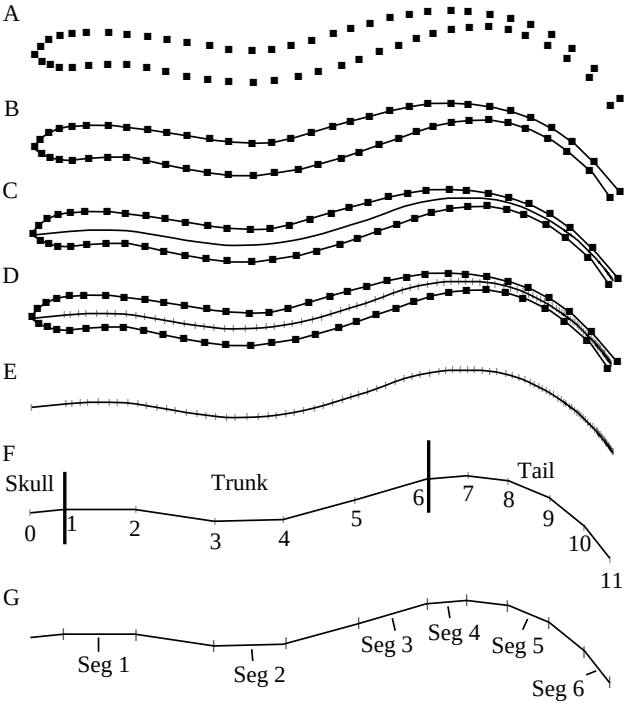

Fig. 1. Series of illustrations demonstrating the process of image analysis. (A) Ventral images of swimming salamanders were first digitized by marking a series of coordinates defining the outline of the animal's body. (B) A series of cubic splines was then generated using a computer to connect the coordinates, creating an outline. (C) A midline to this outline was then calculated. (D,E) The positions of axial skeletal elements (determined from X-ray photographs) were then superimposed upon the midline. (F) The patterns of movement of 12 points (points 0–11) distributed along the length of the body were analyzed. (G) In addition, movements of six segments (Seg) distributed along the length of the body were also analyzed.

Materials and methods

Animals

Morphological and kinematic data were collected from four *Siren intermedia* Le Conte [33.7–38.1 cm total length (*L*), mean 36.3 cm]. Animals were kept individually in 40 l aquaria and were maintained on a diet of earthworms (*Lumbricus* sp.). Water temperature within aquaria was kept at 19.5±1.5 °C and a photoperiod of 12 h:12 h light:dark was established.

Experimental procedures

Salamanders were video-taped at 200 fields s^{-1} swimming in a flow tank (working section 28 cm×28 cm×78 cm) at five velocities: 0.3, 0.45, 0.6, 0.9 and 1.5 lengths s^{-1} ($L\,s^{-1}$) using a NAC high-speed video system. These velocities (0.3–1.5 $L\,s^{-1}$) span the range in which *S. intermedia* could hold its position in the flow for several tailbeat cycles. Steady swimming sequences (variation in swimming speed less than 10 % among tailbeats) at the highest speed proved difficult to obtain, and for one individual the highest speed was actually 1.85 $L\,s^{-1}$ rather than 1.5 $L\,s^{-1}$. As a result, these data will be analyzed separately from the high-speed data from the other individuals. A camera aimed at a front surface mirror angled at 45 ° below the working section of the flow tank was used to record a ventral view of the swimming animal. In addition, one individual was video-taped from a lateral view at all speeds to ensure that the body remained in a horizontal plane during all sequences to be used for analysis. As *S. intermedia* typically swam voluntarily near the bottom of the tank, the lateral view was not recorded for other individuals, and sequences in which the animal was not swimming within a horizontal plane along the bottom of the tank were not used for analysis.

As fluid flow along the bottom of the flow tank is different from that in the central portion due to boundary effects (Vogel, 1983), flow speed was calibrated using dye injections 0.5–1.0 cm from the bottom of the tank. Calibration curves were calculated from this location and were repeatable. Gap-span ratios (Webb, 1993) were calculated for one individual at all speeds in order to determine whether the side walls of the flow tank were significantly influencing the swimming behavior of the animal. Gap-span ratios at all speeds suggested that side wall effects were negligible during swimming trials.

Four tailbeat cycles were video-taped for each individual at each of the five swimming speeds (in total, 80 cycles were recorded). While all four tailbeat cycles for each individual at

every speed could not always be collected consecutively (as *S. intermedia* typically did not hold their position well in the flow during swimming), slightly over half of the sequences included four consecutive tailbeats, while the other sequences consisted of two sets of two consecutive tailbeats. Twenty video fields per tailbeat cycle were analyzed, in addition to five video fields before the start of the first cycle and five fields after the end of the last cycle.

Image analysis

Video fields of each locomotion sequence were digitized by marking and collecting the Cartesian coordinates of 63 points around the *S. intermedia* outline in ventral view (Fig. 1A). A custom-designed program (described in detail by Jayne and Lauder, 1993, 1995) was then used to fit a series of cubic splines connecting the digitized points along each side of the outline (Fig. 1B). The construction of the animal's midline was then completed by defining a series of points exactly intermediate to the left and right halves of the digitized outline in coordinate space (Fig. 1C). The midline was then divided into segments, each of which corresponded to an element of the animal's axial skeleton (Fig. 1D,E). Division of the midline was performed by first taking an X-ray photograph of each animal (Fig. 2). Every X-ray photograph was then digitized to find the lengths of each axial element, from the skull to the last caudal vertebra. Absolute lengths of all skeletal elements were then converted to relative lengths per individual, and these relative lengths were used to divide the midlines. All axial segments are calculated by the program as a straight-line function, and the coordinates that define the beginning and end of each element are known. In addition, the angle of bending (flexion) between every two consecutive elements was calculated.

In order to characterize axial movements along the entire body, 12 midline points were analyzed for each individual at every speed: the tip and base of the skull (points 0 and 1), four points approximately evenly divided along the trunk (points 2–5), the cloaca, or the point at which the tail originates (point 6), four points approximately evenly divided along the tail (points 7–10) and the caudal tip of the tail (point 11) (Fig. 1F; Table 1). These points were chosen because they divided the animal's trunk and tail into equal numbers of segments (five of similar size within each region), plus one segment defining the skull.

Kinematic variables

The maximum lateral displacement (z_{max}) of each of the 12 midline points was calculated for all tailbeat cycles as the average distance traveled between the extreme lateral excursions of each cycle, divided by two (Fig. 3B). As an intervertebral joint on an undulating body becomes laterally displaced to one side, it also becomes flexed concave to the opposite side. Maximum flexion (B_{max}) between adjacent axial

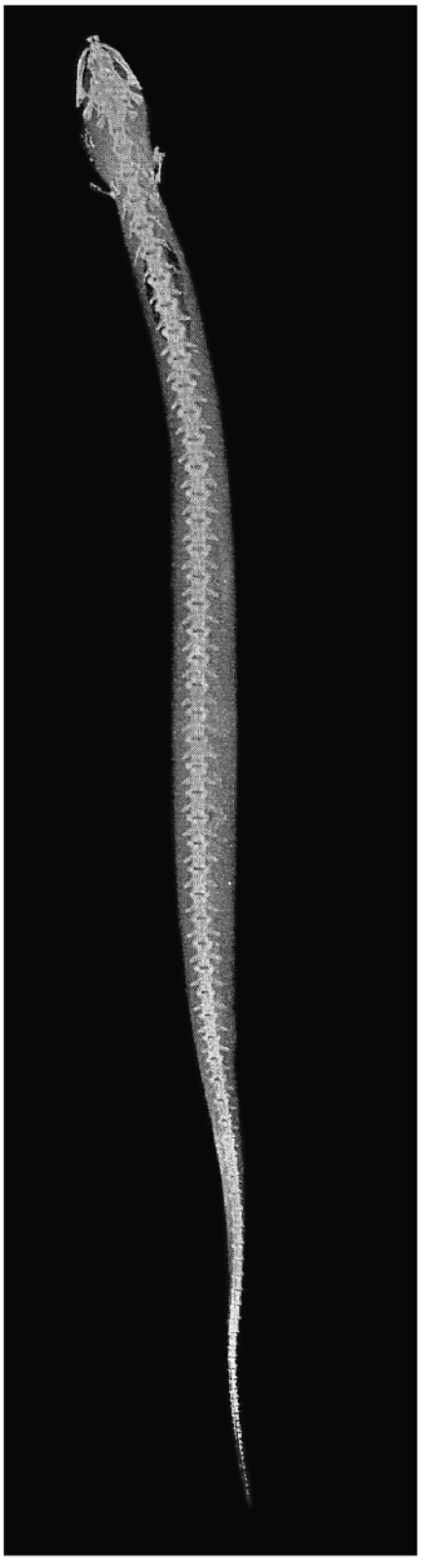

Fig. 2. X-ray photograph of a sirenid salamander, *Siren intermedia*, showing changes in the size and shape of axial elements along the vertebral column. Note that the tail is laterally compressed and that tail vertebrae become smaller distally. The most distal tail vertebrae are so small that they do not appear clearly in this figure, although they are apparent on the X-ray photograph itself when it is backlit. This individual was not one of the four individuals used in this study (but this individual was small enough to stretch out on a single piece of X-ray film).

Table 1. *Longitudinal positions of 12 analyzed sites along body in terms of absolute distance from tip of snout, relative distance from tip of snout, and axial skeletal element number (axial element 1 is the skull, and all other axial elements are vertebrae, numbered antero-posteriorly)*

	Absolute distance along body (cm)				Relative distance along body (%*L*)				Axial location (element number) (between two axial elements, or at tip of snout or tail)			
	Individual				Individual				Individual			
Site	1	2	3	4	1	2	3	4	1	2	3	4
0	0	0	0	0	0	0	0	0	Anterior tip of skull			
1	2.2	1.9	2.1	2.0	5.9	5.4	5.7	6.0	1–2	1–2	1–2	1–2
									Base of skull			
2	7.2	6.0	6.7	5.8	19.0	17.0	17.9	17.2	9–10	9–10	9–10	9–10
3	12.4	10.6	11.4	10.2	32.5	29.8	30.1	30.4	16–17	17–18	16–17	17–18
4	16.7	14.6	15.4	14.2	43.8	41.1	40.7	42.0	22–23	24–25	22–23	24–25
5	21.6	19.1	19.9	18.0	56.8	53.7	52.8	53.3	29–30	32–33	29–30	31–32
6	26.8	23.2	24.7	22.0	70.5	65.3	65.4	65.1	37–38	40–41	37–38	39–40
									Base of tail (cloaca)			
7	29.2	25.5	27.2	24.4	76.8	71.8	72.0	72.4	41–42	45–46	42–43	45–46
8	31.3	28.0	29.8	26.5	82.3	78.8	79.0	78.7	45–46	51–52	49–50	51–52
9	33.7	30.5	32.5	29.0	88.4	85.8	86.2	86.0	51–52	59–60	58–59	59–60
10	35.8	33.2	35.1	31.4	94.1	93.2	92.9	92.9	59–60	72–73	71–72	71–72
11	38.1	35.6	37.8	33.7	100	100	100	100	75	97	95	95
									Posterior tip of tail			

L, total length.
Segment 1, sites 1–2; segment 2, sites 3–4; segment 3, sites 5–6; segment 4, sites 6–7; segment 5, sites 8–9; segment 6, sites 10–11.

skeletal elements was calculated for points 1–10 (Fig. 1F) as the average angular excursion between points of extreme flexion, divided by two (Fig. 3C). Previous workers have found that, during swimming, maximal displacement to one side and maximal flexion (concave to the opposite side) at a given longitudinal position do not necessarily coincide in time in some centrarchid fishes (e.g. Jayne and Lauder, 1993, 1995). Therefore, at the 10 points used for calculating flexion, the difference in timing, or phase lag (*z*–*B* lag) between maximal displacement to one side and maximal flexion, concave to the opposite side, was calculated (Fig. 3). All phase lags were calculated as a proportion of a tailbeat cycle. A positive *z*–*B* lag indicates that maximum displacement occurred prior to maximum flexion, whereas a negative lag indicates that flexion occurred before displacement (note that the phase lag notation used here is different from that used in Jayne and Lauder, 1995).

Maximum path angle of each point was also calculated for each tailbeat cycle (Fig. 3A). The path of a point was defined as the straight line connecting the positions of that point between any two consecutive video fields. Path angle was then defined as the angle subtended by the path relative to the direction of forward travel. Phase lags between maximum lateral displacement and maximum path angle (*z*–path lag) were also calculated (Fig. 3).

Tailbeat cycle time (period) was calculated as the average time taken by the tip of the tail to undergo one undulatory cycle. Tailbeat frequency was calculated as the inverse of tailbeat period.

In addition, an analysis of the orientation and movement of larger body segments (Fig. 1G) was carried out. Analyses of undulatory locomotion are often simplified by describing an undulating body as a series of interconnected linear segments (see Gray, 1933). Although the image analysis methods used in the present study divided the salamander's midline into as many linear segments as there are axial skeletal elements, these 75–97 axial segments were reduced to 11 linear segments, one corresponding to the skull, five defining the trunk (of approximately equal length) and five defining the tail (smaller than the trunk segments, but of approximately equal length amongst themselves) (Fig. 1F). Each of these segments consists of different numbers of vertebrae (Table 1), as axial elements change in length longitudinally (Fig. 2; see also Fig. 5).

Six of these larger segments (three along the trunk and three along the tail; Fig. 1G) were used to analyze variations in the interactions between body segments and the surrounding fluid environment at different longitudinal positions and at different swimming speeds. The lateral velocity of each segment was calculated at all swimming speeds between all digitized video fields by determining the distance traveled by the midpoint of the segment in the lateral (*z*) dimension between any two consecutively sampled video fields (spaced 1/20th of a tailbeat cycle apart) and dividing that by the time elapsed. The average

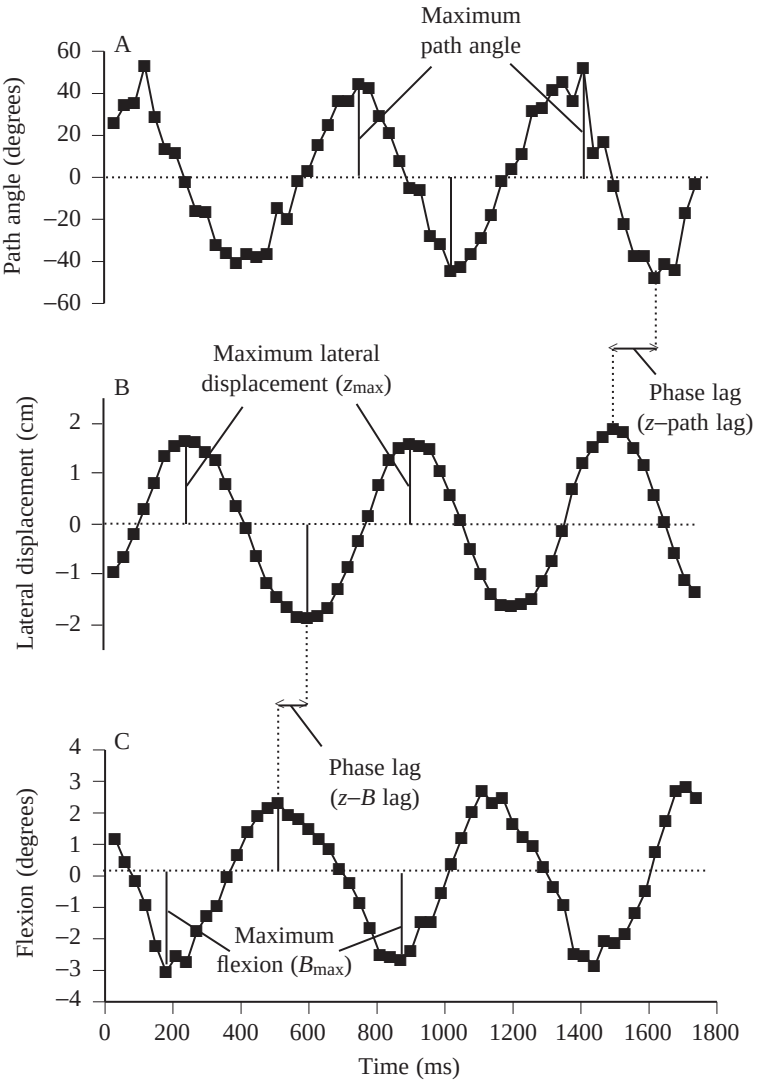

Fig. 3. Plots of three kinematic variables, (A) path angle, (B) lateral displacement and (C) flexion, *versus* time for position 8 (see Fig. 1F) during several tailbeat cycles from one individual. Movement to the right or flexion concave to the right is designated with a positive sign, whereas movement or flexion to the left is designated with a negative sign. Maxima for these variables were calculated as the average absolute distance between maximal excursions to the right and to the left, divided by two. Phase lags between maximum lateral displacement to one side, maximum path angle and maximum flexion concave to the other side were also determined as shown. Note that maximum flexion tends to occur slightly before maximum displacement and that the maximum path angle always occurs approximately one-quarter of a cycle after maximum displacement.

maximum lateral velocity of each segment was then calculated for all tailbeat cycles. The orientation (θ) or the angle subtended by each segment relative to the direction of forward travel was calculated for all six segments at all swimming speeds for all digitized video fields (Fig. 4), and the maximum orientation was determined for each tailbeat cycle. The maximum path angle of each segment was also calculated for all cycles. The path of a segment was defined as the straight line connecting the midpoint of that segment between any two consecutive video fields, and path angle was again defined as the angle subtended by the path relative to the direction of forward travel (Fig. 4). The relative timing of these three events (maximum lateral velocity, θ, and path angle) within a tailbeat cycle was determined by calculating the phase lag between maximum lateral displacement of a segment (its midpoint) and each of the three variables for all tailbeat cycles.

The angle of attack (α) of three tail segments (segments 4, 5 and 6, Fig. 1G) was also calculated for all digitized video fields at all speeds. The angle of attack of a tail segment is the difference between θ and the path angle of that segment (Fig. 4). The angle of attack is defined as negative whenever the segment itself is oriented at a larger angle (θ) to the flow than is the path angle, assuming they are both of the same sign; i.e. both oriented either to the left or to the right of the animal's direction of travel. The angle of attack is positive when the path angle is greater than θ.

For all sequences, the speed of the mechanical wave traveling along the body was measured between points 2 and 11 (Fig. 1F). Average wave speed was calculated by taking the distance (along the body) between points 2 and 11 and dividing that by the time lag between maximum displacement at these points. Multiple calculations of wave speed were possible within each locomotor sequence. To examine whether wave speed changed with longitudinal position, the distance along the body between points 2 and 6 and the time lag between maximum lateral displacement at these points were used to calculate wave speed along the trunk, while the distance and time lag between points 6 and 11 were used to calculate wave speed along the tail.

For one individual, propulsive wavelengths were calculated for all swimming speeds. Following Webb *et al.* (1984), half-wavelengths were measured by superimposing the *x*-

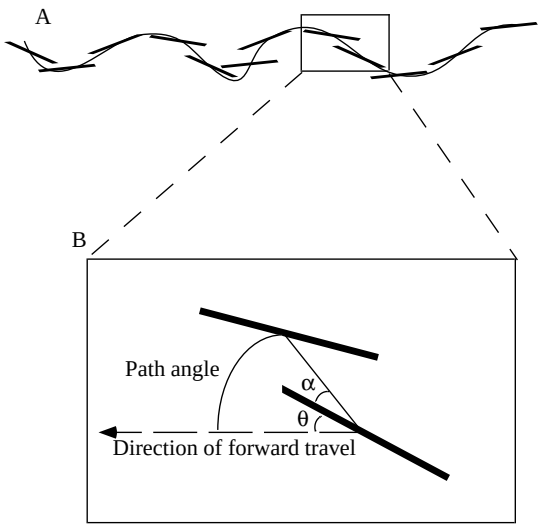

Fig. 4. (A) The position of a tail segment at equally spaced time intervals along its path of travel over several tailbeat cycles. (B) The kinematic variables θ (orientation), path angle and α (angle of attack). The orientation (θ) of a segment is the angle subtended by that segment relative to the direction of forward travel. Path angle is the angle between the direction of forward travel and a straight line connecting the midpoint of a segment between consecutive analyzed video fields. The angle of attack (α) is the difference between the path angle and the orientation angle and is positive if the path angle is more extreme than θ, as shown in B.

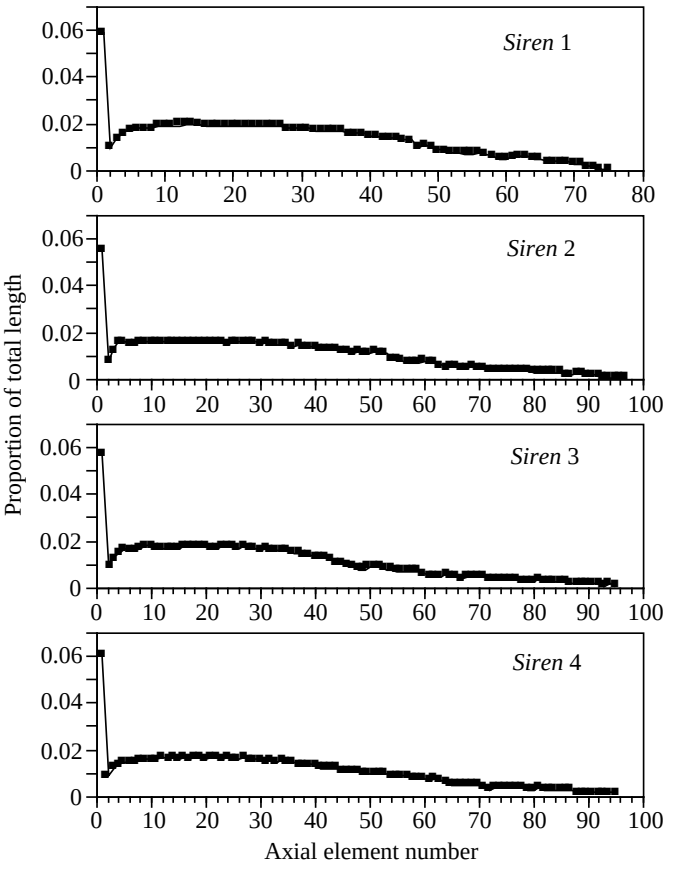

Fig. 5. Graphical representation of the lengths of axial skeletal elements in each of the four salamanders used. Note that, although individual 1 has substantially fewer axial elements (which are accordingly relatively larger, in general), the overall pattern of how the axial elements change size with longitudinal position is quite similar across the four individuals.

coordinates of the tip of the snout from *S. intermedia* midlines at the start of successive tailbeats (180° out of phase). A digitizing program was then used to measure the length (in cm) of each of the half-waves along the body. These half-wavelengths could then be multiplied by two to get the propulsive wavelength. Propulsive wavelength could also be multiplied by undulatory frequency to estimate the speed of the mechanical wave.

Finally, using the reactive model of Lighthill (1975), total power output, energy lost to the wake, thrust power output and Froude efficiency were estimated for one individual swimming at speeds between 0.3 and $1.5\,L\,s^{-1}$. In addition, these same parameters were estimated for the individual performing the high-speed ($1.85\,L\,s^{-1}$) sequence.

Statistical analyses

In addition to the calculation of basic statistics for all kinematic variables described above, several analyses of variance (ANOVAs) were performed using SAS (Statistical Analysis System) to test for the effects of swimming speed and longitudinal position on these variables. To examine the effects of swimming speed and body position on maximal displacement, flexion, path angle and their relative timing with respect to one another, a three-way mixed-model ANOVA was performed (Sokal and Rohlf, 1981). Both swimming speed and longitudinal position were considered as fixed effects, while individual was considered a random effect. The effects of longitudinal position and swimming speed on the mechanical wave speed, the maximum lateral velocity, the path angle and the orientation (θ) of body segments were also tested using three-way mixed-model ANOVAs. Additionally, a final three-way mixed-model ANOVA was used to test for the effects of swimming speed and longitudinal position on the magnitude of positive and negative angles of attack of the three tail segments. A two-way mixed-model ANOVA was used to analyze tailbeat period and frequency, with speed as a fixed effect and individual as a random effect.

For all ANOVAs, the fixed effects were tested over their respective interaction mean square (fixed effect × individual) and the random effect was tested over the error mean square. Interactions among variables were also tested over the appropriate mean square (Zar, 1984).

Whenever there was a significant difference among levels within a fixed effect for a particular kinematic variable, Tukey *post-hoc* tests were used to determine specifically which levels differed from one another. In addition, as one individual had significantly fewer vertebrae than the others, I also determined whether this individual had significantly different kinematic patterns from those of the other individuals. To do this, I used

Tukey *post-hoc* tests to determine differences among individuals (random effect) whenever a kinematic variable showed significant interindividual variation. Although, typically, one does not perform *post-hoc* tests on a random effect, this seemed a reasonable way to determine whether this particular individual deviated kinematically from the rest. To account for multiple simultaneous ANOVAs, the level of statistical significance was adjusted within each table (Tables 2, 4) using the sequential Bonferroni technique described by Rice (1989).

Results

Morphology

As shown in Fig. 1F, the axial skeleton of a salamander can be divided into three distinct regions, the skull, the trunk (from the base of the skull to the cloaca) and the tail (from the cloaca to the posterior tip of the tail). The skull makes up 5–6 % of the animal's total length (Table 1). The trunk makes up 59–65 %*L* (Table 1) and is approximately circular in cross section. The trunk is relatively narrow anteriorly, where the two reduced forelimbs are present (approximately 2 cm posterior to the base of the skull). The trunk then widens posterior to the limbs to a maximum diameter of approximately 7 %*L*, and gradually becomes smaller posteriorly until its diameter is only 4–5 %*L* at the base of the tail (similar to the trunk diameter at the origin of the forelimbs). The tail makes up 29–35 %*L* (Table 1). Tail depth is approximately 5 %*L* along most of its length but tapers near the tip. The tail also becomes more laterally compressed posteriorly.

There are 94–96 vertebrae in three of the individuals, while the fourth individual has only 74, although it is the longest in total length (Table 1). Axial elements consistently vary longitudinally in size and shape in *S. intermedia* (Figs 2, 5). While the skull makes up 5–6 %*L*, individual vertebrae vary in length from 0.1 to 2.0 %*L*, depending upon longitudinal position and individual (the individual with only 74 vertebrae had relatively larger vertebrae). The first three vertebrae are small and increase in size sequentially. The rest of the vertebrae within the trunk are relatively larger and are of similar size. Moving posteriorly along the tail, the vertebrae steadily decrease in size and are smallest at the tip. Despite the fact that one individual has fewer vertebrae than the other three, the pattern of longitudinal variation in vertebral size is similar across all individuals (Fig. 5).

Kinematics

At all speeds, most points along the axial skeleton move in wave-like cycles, being displaced laterally from side to side in a periodic fashion (e.g. Fig. 3). Only the most anterior points 0 and 1 (tip and base of skull) do not show a consistent wave-like pattern of lateral displacement (except at 1.5 and 1.85 $L\,s^{-1}$). There is a significant effect ($P<0.001$) of longitudinal position on the maximum lateral displacement (z_{max}) of points along the vertebral column (Table 2). Lateral displacement is always highest at the tip of the tail (site 11) and tends to be lowest at the anterior tip of the skull (site 0) although, at the highest speeds, z_{max} is smallest at or just posterior to the base of the skull (sites 1 or 2) (Fig. 6A). Speed, although not having a statistically significant effect on the

Table 2. *Results from a three-way ANOVA of the effects of longitudinal position (site), swimming speed and individual on kinematic variables associated with 12 points along the body*

Variable	Site	Speed	Individual	Site × Speed	Site × individual	Speed × individual	Site × speed × individual
z_{max}	270.4** (11, 33)	3.1 (4, 11)	24.2** (3, 671)	4.5** (44, 121)	4.5** (33, 671)	32.3** (11, 671)	0.6 (121, 671)
B_{max}	8.7** (9, 27)	0.6 (4, 11)	32.2** (3, 560)	1.6 (36, 99)	18.9** (27, 560)	26.8** (11, 560)	7.4** (98, 560)
Maximum path angle	218.0** (11, 33)	2.2 (4, 11)	21.5** (3, 671)	4.8** (44, 121)	7.0** (33, 671)	31.6** (11, 671)	2.3** (121, 671)
z–*B* lag	4.3* (9, 27)	8.8* (4, 11)	4.3 (3, 542)	3.6** (36, 96)	4.6** (27, 542)	1.6 (11, 542)	1.6* (96, 542)
z–path lag	12.8** (11, 33)	2.8 (4, 11)	4.4 (3, 605)	1.6 (44, 104)	1.8 (33, 605)	1.8 (11, 605)	1.2 (104, 605)
B–path lag	4.5* (9, 27)	7.3 (4, 11)	8.0** (3, 535)	4.0** (36, 93)	3.9** (27, 535)	2.2 (11, 535)	1.3 (93, 535)

Degrees of freedom are given in parentheses.

Table entries are *F*-values.

Significance: *$P\leqslant0.05$, **$P\leqslant0.005$, using the sequential Bonferroni method described in Rice (1989).

z_{max}, maximum lateral displacement; B_{max}, maximum flexion; *z*–*B* lag, phase lag between z_{max} and B_{max}; *z*–path lag, phase lag between z_{max} and maximum path angle; *B*–path lag, phase lag between B_{max} and maximum path angle.

See Fig. 3 for further details.

Table 3. *Mean phase lags (measured as a proportion of a tailbeat cycle) between maximum lateral displacement and maximum flexion, and between maximum lateral displacement and maximum path angle*

Longitudinal position	*z*–*B* lag					*z*–path lag				
	Swimming speed ($L\,s^{-1}$)					Swimming speed ($L\,s^{-1}$)				
	0.3	0.45	0.6	0.9	1.5	0.3	0.45	0.6	0.9	1.5
0	No flexion at position 0					0.29 (0.04)	0.16 (0.03)	0.10 (0.03)	0.20 (0.01)	0.21 (0.03)
1	0.06 (0.04)	–0.20 (0.03)	0.00 (0.03)	–0.15 (0.05)	0.05 (0.06)	0.21 (0.04)	0.22 (0.02)	0.13 (0.02)	0.22 (0.04)	0.20 (0.02)
2	–0.14 (0.03)	–0.14 (0.02)	–0.15 (0.02)	–0.10 (0.01)	–0.09 (0.02)	0.26 (0.02)	0.24 (0.02)	0.21 (0.02)	0.20 (0.02)	0.21 (0.01)
3	–0.07 (0.02)	–0.09 (0.02)	–0.08 (0.01)	–0.08 (0.01)	–0.03 (0.01)	0.27 (0.03)	0.22 (0.02)	0.23 (0.01)	0.21 (0.01)	0.20 (0.02)
4	–0.11 (0.02)	–0.08 (0.01)	–0.06 (0.01)	–0.06 (0.01)	–0.05 (0.00)	0.21 (0.03)	0.22 (0.02)	0.23 (0.01)	0.23 (0.02)	0.26 (0.01)
5	–0.11 (0.01)	–0.10 (0.00)	–0.08 (0.01)	–0.09 (0.01)	–0.08 (0.01)	0.26 (0.02)	0.22 (0.01)	0.26 (0.01)	0.24 (0.01)	0.26 (0.01)
6	–0.12 (0.01)	–0.11 (0.01)	–0.11 (0.01)	–0.12 (0.01)	–0.12 (0.02)	0.24 (0.02)	0.23 (0.01)	0.24 (0.01)	0.24 (0.01)	0.26 (0.01)
7	–0.14 (0.01)	–0.14 (0.01)	–0.13 (0.01)	–0.16 (0.02)	–0.14 (0.02)	0.24 (0.01)	0.26 (0.01)	0.24 (0.01)	0.21 (0.03)	0.22 (0.01)
8	–0.10 (0.02)	–0.16 (0.02)	–0.16 (0.01)	–0.14 (0.01)	–0.14 (0.01)	0.30 (0.02)	0.23 (0.01)	0.23 (0.01)	0.22 (0.01)	0.22 (0.01)
9	–0.18 (0.01)	–0.21 (0.01)	–0.18 (0.02)	–0.12 (0.02)	–0.05 (0.03)	0.20 (0.02)	0.20 (0.01)	0.19 (0.01)	0.20 (0.01)	0.19 (0.01)
10	–0.19 (0.02)	–0.19 (0.02)	–0.18 (0.03)	–0.07 (0.02)	–0.10 (0.03)	0.19 (0.01)	0.16 (0.01)	0.16 (0.01)	0.16 (0.01)	0.17 (0.01)
11	No flexion at position 11					0.17 (0.02)	0.14 (0.02)	0.10 (0.00)	0.14 (0.01)	0.16 (0.01)

Values are means with S.E.M. in parentheses.

L, total length.

z–*B* lag, phase lag between maximum lateral displacement, *z*, and maximum flexion; *z*–path lag, phase lag between z_{max} and maximum path angle.

maximum amplitude of lateral displacement (P=0.06; Table 2), does appear to have a biologically real effect on this variable as lateral displacement tends to increase with speed, particularly in the middle regions of the body (Fig. 6A).

Maximum intervertebral flexion also varies significantly with longitudinal position (P<0.001; Table 2). Along much of the body, maximum flexion ranges from 1 to 4 ° although, at the base of the skull, flexion can reach 7–10 ° at the highest speeds (Fig. 6B). Speed, however, does not have a statistically significant effect on maximal flexion (P=0.65; Table 2), although graphical representation of the data suggests that flexion tends to increase with speed along the anterior portion of the body (sites 1–4), while decreasing with speed along the posterior regions of the tail, except for the single trial at $1.85\,L\,s^{-1}$, which was not included in the statistical analysis (Fig. 6B).

Maximum lateral displacement and maximum intervertebral flexion do not coincide in time with one another. At a given longitudinal site, maximal flexion typically occurs before maximal displacement (i.e. negative *z*–*B* lag), and this phase lag changes significantly in duration depending upon swimming speed (P<0.05) and longitudinal position (P<0.05; Tables 2, 3). Along most of the body, the *z*–*B* phase lag ranges from –0.05 to –0.19 tailbeat cycles. However, near the base of the skull, this phase lag is quite variable owing to the low and inconsistent undulatory displacement at this location, which makes it difficult to pick clear points in time at which this site is maximally laterally displaced or flexed.

There is also a significant effect of longitudinal position on the maximum path angle of points along the body moving through the water (P<0.001; Table 2). Maximum path angle is usually lowest at the tip of the snout (except at 1.5 and $1.85\,L\,s^{-1}$) and is always highest at the tip of the tail, where it can even exceed 90 ° (Fig. 6C). Speed did not have a statistically significant effect on this variable (P=0.13; Table 2), although path angle appeared to decrease with speed along the tail (Fig. 6C).

There is significant individual variation for maximum lateral displacement, flexion and path angle. Tukey *post-hoc* tests

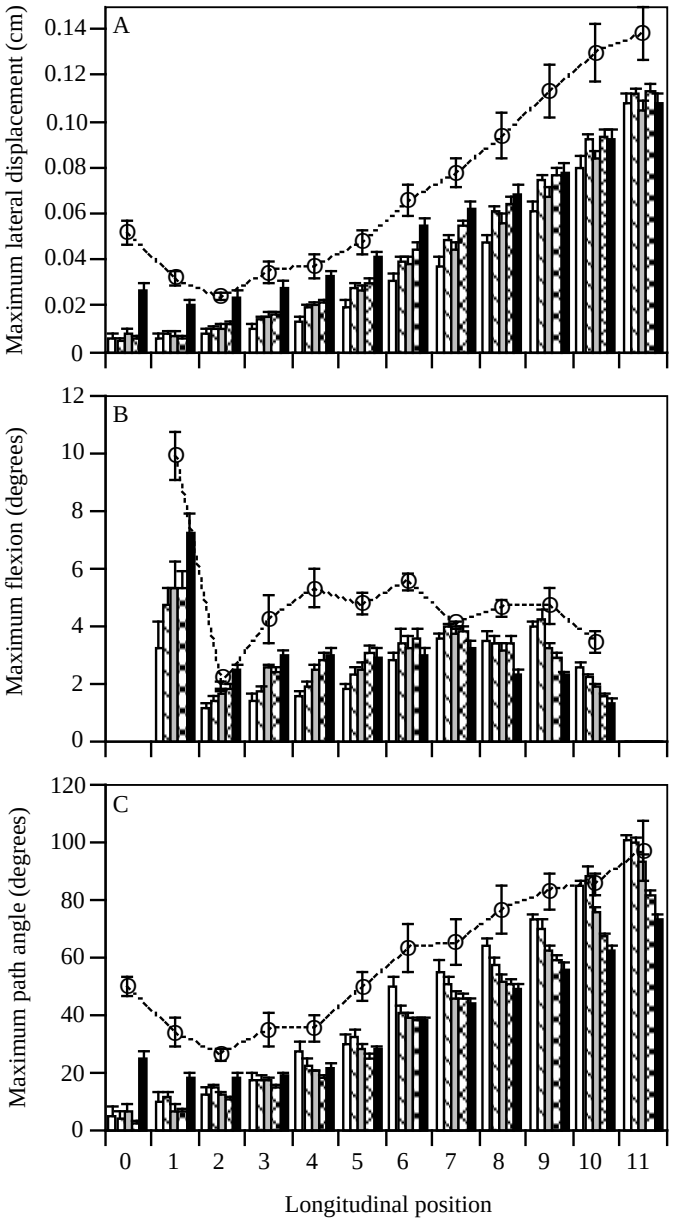

Fig. 6. Graphs of average maximum lateral displacement z_{max} (A), maximum flexion B_{max} (B) and maximum path angle (C) for 12 points along the body at all swimming speeds and from all individuals. Vertical bars represent the five swimming speeds, 0.3, 0.45, 0.6, 0.9 and $1.5\,L\,s^{-1}$ (where L is body length) from left to right at each position, while the open circles represent the average values from one individual swimming at $1.85\,L\,s^{-1}$. Error bars represent standard errors (S.E.M.).

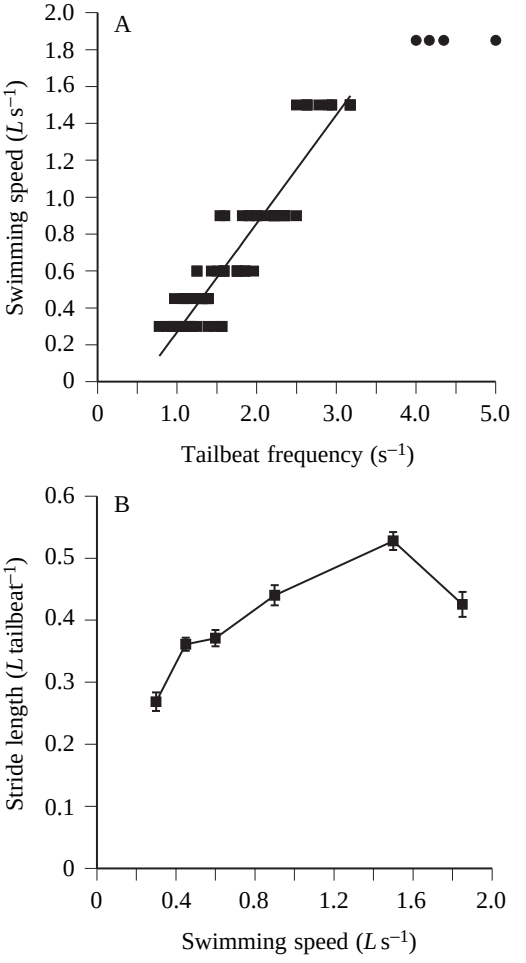

Fig. 7. (A) Swimming speed increases linearly with tailbeat frequency between 0.3 and $1.5\,L\,s^{-1}$ (filled squares). However, inclusion of data from the high-speed swimming sequence at $1.85\,L\,s^{-1}$ (filled circles) reduces the slope of this linear relationship because tailbeat frequency increases disproportionately relative to swimming speed above $1.5\,L\,s^{-1}$. (B) The distance moved per tailbeat (stride length), measured as a proportion of the salamander's length (L), increases with swimming speed between 0.3 and $1.5\,L\,s^{-1}$, but begins to decrease at the highest swimming speed. Error bars represent standard errors (S.E.M.).

reveal that one individual typically differs from the other three individuals in terms of these kinematic variables, although it is not the individual with substantially fewer vertebrae. This individual's differences are probably due to its mode of swimming at the lowest speed where it used obvious undulations of the anterior portion of the body whereas the other individuals tended not to undulate their snouts at these low swimming speeds. Concomitant with this increased anterior undulation were increased anterior flexion and path angle, causing this individual to stand out from the rest kinematically. The unique kinematic patterns of this individual at slow speeds are also likely to be responsible (at least in part) for many of the significant interaction terms in the ANOVAs.

Swimming speed has a significant effect on tailbeat period ($P<0.001$) and frequency ($P<0.001$), with period decreasing significantly and frequency increasing significantly with swimming speed. The relationship between swimming speed and tailbeat frequency (not including data from the individual swimming at $1.85\,L\,s^{-1}$) is best approximated by the straight line $U=0.59f-0.32$ (where U is swimming speed and f is tailbeat frequency; $r^2=0.86$; Fig. 7A). Including data for the highest speed ($1.85\,L\,s^{-1}$) changes this relationship to $U=0.51f-0.19$ ($r^2=0.88$, Fig. 7A). Swimming speed divided by

Table 4. *Results from a three-way ANOVA of the effects of longitudinal position, swimming speed and individual on kinematic variables associated with six segments along the body*

Variable	Longitudinal position	Speed	Individual	Segment × speed	Segment × individual	Speed × individual	Site × speed × individual
Maximum lateral velocity	123.1** (5, 15)	42.6** (4, 11)	36.8** (3, 323)	16.8** (20, 54)	7.8** (15, 323)	11.8** (11, 323)	1.3 (54, 323)
Maximum path angle	295.6** (5, 15)	2.2 (4, 11)	21.6** (3, 328)	3.4** (20, 54)	4.2** (15, 328)	15.5** (11, 328)	1.6 (54, 328)
θ_{max}	202.3** (5, 15)	0.1 (4, 11)	3.3 (3, 333)	13.2** (20, 55)	14.0** (15, 333)	40.2** (11, 333)	2.7** (55, 333)
z–vel lag	22.9** (5, 15)	0.7 (4, 11)	8.1** (3, 307)	0.9 (20, 51)	1.2 (15, 307)	5.5** (11, 307)	1.2 (51, 307)
z–path lag	17.0** (5, 15)	1.0 (4, 11)	2.4 (3, 307)	1.2 (20, 51)	1.4 (15, 307)	3.3* (11, 307)	1.4 (51, 307)
z–θ lag	5.8 (5, 15)	1.0 (4, 11)	9.6** (3, 307)	1.8 (20, 51)	4.9** (15, 307)	9.1** (11, 307)	2.0* (51, 307)

Table entries are *F*-values.

Significance: *$P \leq 0.05$, **$P \leq 0.005$, using the sequential Bonferroni method described in Rice (1989).

Degrees of freedom are given in parentheses.

θ, orientation angle; *z*–vel lag, phase lag between maximum lateral displacement and maximum lateral velocity; *z*–path lag, phase lag between z_{max} and maximum path angle; *z*–θ lag, phase lag between z_{max} and θ_{max}.

tailbeat frequency, or stride length (distance moved per tailbeat cycle), increases from an average of $0.27\,L$ tailbeat^{-1} at a swimming speed of $0.3\,L\,s^{-1}$ to $0.53\,L$ tailbeat^{-1} at a swimming speed of $1.5\,L\,s^{-1}$ and then decreases at $1.85\,L\,s^{-1}$ to $0.42\,L$ tailbeat^{-1} (Fig. 7B).

Analysis of body segments 1–6 revealed that there is a significant effect of longitudinal position on a segment's maximum lateral velocity ($P<0.001$), path angle ($P<0.001$) and orientation (θ) ($P<0.001$; Table 4). Each of these maxima increases posteriorly along the vertebral column (Fig. 8). Swimming speed, however, only had a significant effect on maximum lateral velocity with higher velocities of movement occurring at higher swimming speeds (Fig. 8A). While swimming speed did not statistically significantly affect the path angle or orientation (θ) of segments, it appears that path angle and orientation tend to decrease with speed near the tip of the tail (segment 6; Fig. 8B,C).

The maximum lateral velocity and maximum path angle of a segment are typically reached at a similar time (mean=0.24 cycles after maximum lateral displacement to one side, or as the segment crosses the axis of forward movement; Fig. 9; Table 5). However, this relative timing was significantly affected by longitudinal position, with the most posterior segments tending to reach their maxima relatively sooner within a tailbeat cycle than the more anterior segments (Tables 4, 5). Segments tended to reach their maximum

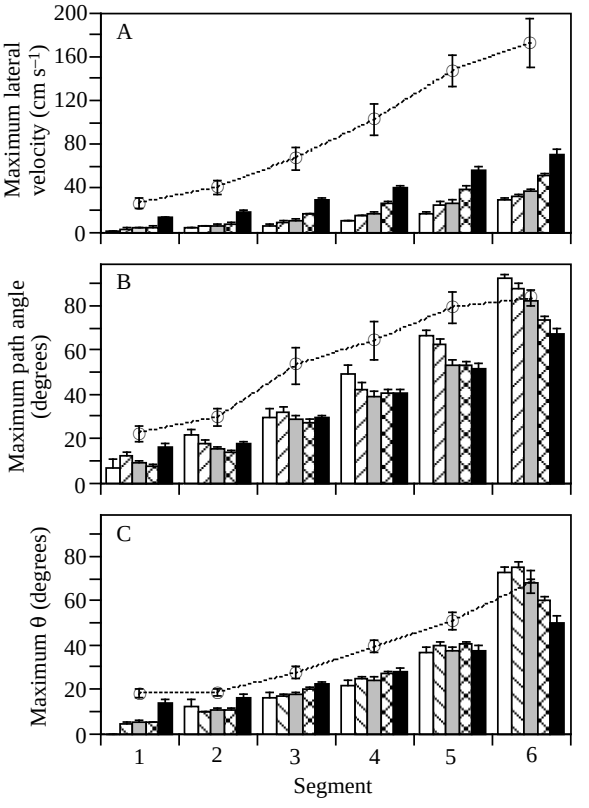

Fig. 8. Graphs of average maximum lateral velocity (A), maximum path angle (B) and maximum orientation (θ) (C) for six linear segments representing different longitudinal portions of the midline of the salamanders (see Fig. 1G) at all swimming speeds and from all individuals. Vertical bars represent the five swimming speeds, 0.3, 0.45, 0.6, 0.9 and $1.5\,L\,s^{-1}$ from left to right at each position, while the open circles represent the average values from one individual swimming at $1.85\,L\,s^{-1}$. Error bars represent standard errors (S.E.M.).

Table 5. *Mean phase lags (proportion of cycle) between maximum lateral displacement (z), maximum lateral velocity (vel), maximum path angle (path) and maximum orientation angle (θ) as a proportion of a tailbeat cycle for six linear segments along the body*

	z–vel lag					*z*–path lag					*z*–θ lag				
	Swimming speed ($L\,s^{-1}$)					Swimming speed ($L\,s^{-1}$)					Swimming speed ($L\,s^{-1}$)				
Segment	0.3	0.45	0.6	0.9	1.5	0.3	0.45	0.6	0.9	1.5	0.3	0.45	0.6	0.9	1.5
1	0.35 (0.05)	0.26 (0.02)	0.25 (0.02)	0.23 (0.01)	0.22 (0.01)	0.31 (0.04)	0.27 (0.02)	0.26 (0.02)	0.22 (0.02)	0.22 (0.01)	0.28 (0.10)	0.16 (0.02)	0.12 (0.03)	0.08 (0.02)	0.21 (0.02)
2	0.27 (0.04)	0.24 (0.01)	0.24 (0.01)	0.25 (0.02)	0.25 (0.01)	0.29 (0.02)	0.21 (0.01)	0.24 (0.01)	0.25 (0.01)	0.24 (0.01)	0.20 (0.02)	0.17 (0.01)	0.20 (0.01)	0.18 (0.01)	0.21 (0.01)
3	0.25 (0.02)	0.28 (0.01)	0.26 (0.01)	0.26 (0.01)	(0.26) (0.01)	0.27 (0.02)	0.26 (0.01)	0.26 (0.01)	0.26 (0.01)	0.28 (0.01)	0.17 (0.02)	0.21 (0.01)	0.21 (0.01)	0.19 (0.01)	0.22 (0.01)
4	0.28 (0.02)	0.27 (0.01)	0.28 (0.01)	0.26 (0.01)	0.28 (0.01)	0.28 (0.01)	0.28 (0.01)	0.27 (0.01)	0.26 (0.01)	0.26 (0.01)	0.22 (0.01)	0.23 (0.01)	0.22 (0.01)	0.21 (0.01)	0.22 (0.01)
5	0.25 (0.02)	0.22 (0.01)	0.23 (0.01)	0.23 (0.01)	0.22 (0.01)	0.24 (0.02)	0.24 (0.01)	0.24 (0.01)	0.24 (0.01)	0.23 (0.01)	0.20 (0.01)	0.18 (0.01)	0.19 (0.01)	0.19 (0.01)	0.19 (0.01)
6	0.22 (0.02)	0.18 (0.01)	0.19 (0.01)	0.21 (0.01)	0.18 (0.01)	0.21 (0.01)	0.19 (0.01)	0.18 (0.00)	0.21 (0.21)	0.20 (0.01)	0.17 (0.01)	0.15 (0.01)	0.13 (0.01)	0.15 (0.01)	0.17 (0.01)

See Fig. 1G for identification of segmental position.
Standard errors (S.E.M.) are given in parentheses.

orientation slightly before reaching maximum velocity and maximum path angle (mean=0.19 cycles after maximum lateral displacement), and this relationship was not significantly affected by longitudinal position.

The angle of attack of the three tail segments (segments 4–6) was analyzed for all speeds and individuals. Regardless of speed, all tail segments spend a proportion of each tailbeat cycle (typically 0.12–0.25 of the cycle) with a negative angle of attack (Fig. 10A). Negative angles of attack usually occur when segments have relatively low path angles, i.e. when segments are near their maximum lateral displacement to either side (Figs 9, 11). The degree to which α becomes negative is not significantly affected by longitudinal position or swimming speed. However, more caudal segments tend to be oriented with more negative values of α, and at lower swimming speeds average values of α also tend to be more negative (Table 6). When α is not negative, the degree to which it is positively oriented is significantly affected by swimming speed ($P<0.05$) such that positive values of α tend to be greater at slower swimming speeds (Table 6). In fact, at the slowest swimming speed, all three tail segments spend between 25 and 40 % of each tailbeat cycle oriented such that α is greater than 20 ° (Fig. 10B). While positive values of α are not significantly affected by longitudinal position, there is a trend for more caudal segments to have greater values (Fig. 10B; Table 6).

The speed of the mechanical wave traveling along the body increases significantly with swimming speed ($P<0.001$)

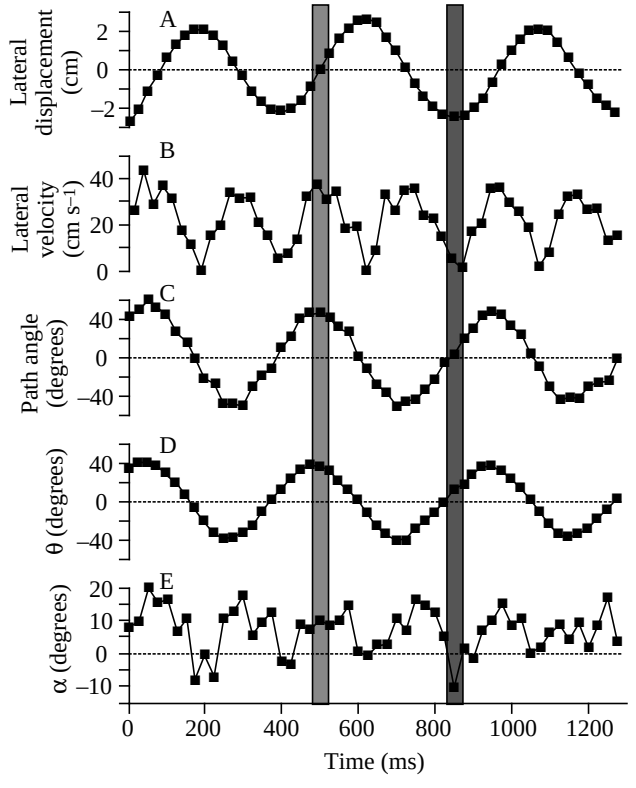

Fig. 9. Plots of lateral displacement (A), lateral velocity (B), path angle (C), orientation θ (D) and angle of attack α (E) of the middle tail segment (segment 5) of one individual during three undulatory cycles at $0.9\,L\,s^{-1}$. The light gray box highlights a period during which this segment crosses the axis of forward progression. Note that at this time the segment is at its maximum lateral velocity and maximum path angle, is just past its maximum orientation, and that its angle of attack is positive. The dark gray box highlights a time at which the segment is maximally displaced to the left. At this time, the segment's lateral velocity is at its lowest, its path angle is near zero, its orientation has just passed zero and its angle of attack is negative.

Table 6. *Mean negative and positive values of the angle of attack α for three linear segments along the tail*

	Average value of negative α					Average value of positive α				
	Swimming speed ($L\,s^{-1}$)					Swimming speed ($L\,s^{-1}$)				
Segment	0.3	0.45	0.6	0.9	1.5	0.3	0.45	0.6	0.9	1.5
4	–5.34	–3.58	–3.49	–3.26	–3.91	15.37	12.82	10.05	9.35	8.49
	(0.70)	(0.42)	(0.48)	(0.28)	(0.51)	(0.58)	(0.46)	(0.31)	(0.33)	(0.32)
5	–5.50	–4.92	–4.18	–4.37	–3.81	19.52	16.05	13.06	10.28	9.41
	(0.56)	(0.45)	(0.36)	(0.40)	(0.50)	(0.70)	(0.56)	(0.45)	(0.35)	(0.37)
6	–10.14	–6.77	–7.29	–6.08	–5.18	20.90	16.57	15.28	13.12	12.73
	(0.94)	(0.53)	(0.62)	(0.50)	(0.71)	(0.74)	(0.65)	(0.51)	(0.39)	(0.47)

See Fig. 1G for segmental position.
Standard errors (S.E.M.) are given in parentheses.

(Fig. 12). In addition, the mechanical wave speed varies significantly along the body (P=0.0035); while this trend of wave speed changing along the body is not seen at the three lower speeds, at higher speeds it is clear that the wave travels faster along the tail than along the trunk (Fig. 12A). The ratio of forward swimming speed to average mechanical wave speed increased from 0.44 to 0.68 as swimming speed increased from 0.3 to $1.5\,L\,s^{-1}$. However, during the individual trial at $1.85\,L\,s^{-1}$, this ratio decreased to 0.56 (Fig. 12B).

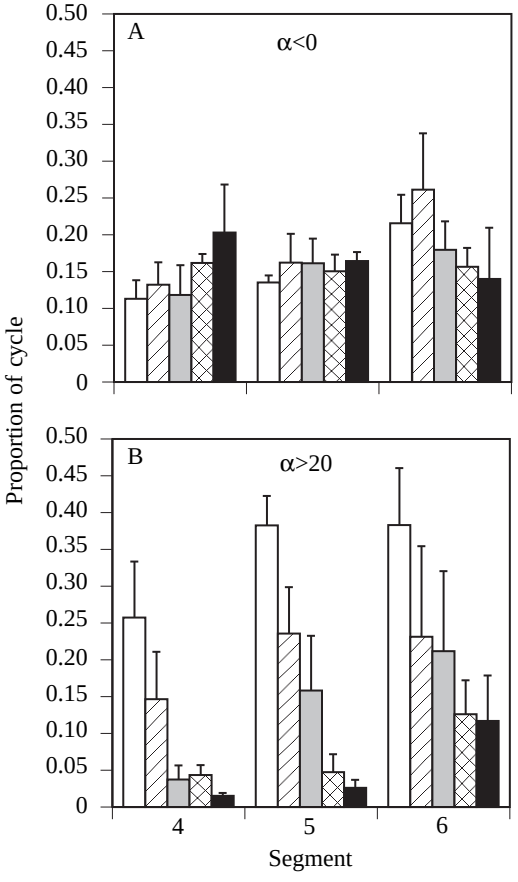

Fig. 10. Bar graphs showing the average proportion of a tailbeat cycle during which three segments along the tail (segments 4, 5 and 6, see Fig. 1G) subtend angles of attack that are negative (A) and greater than (B) 20 °. Bars represent speeds of 0.3, 0.45, 0.6, 0.9 and $1.5\,L\,s^{-1}$ from left to right at each position. Note that tail segments consistently have some proportion of each undulatory cycle during which the angle of attack is negative regardless of swimming speed. Also notice the strong effect that swimming speed has on the proportion of an undulatory cycle during which segments have angles of attack greater than 20 °. Error bars represent standard errors (S.E.M.).

Values of propulsive wavelength ranged from 0.46 to $0.82\,L$ when half-waves were used for the calculation and from 0.56 to $0.79\,L$ when full wavelengths were used. Average propulsive wavelength does not vary significantly with speed and has a mean value of $0.64\,L$. When average propulsive wavelength was used to estimate the average speed of the mechanical wave, values were comparable to those calculated by measuring wavecrest propagation ($\pm 2\,cm\,s^{-1}$), except at $1.5\,L\,s^{-1}$ where the use of average propulsive wavelengths underestimated wave speed by approximately $10\,cm\,s^{-1}$.

The total power generated during swimming determined using Lighthill's reactive model ranged from $4.9\times10^{-4}\,J\,s^{-1}$ to $99.5\times10^{-4}\,J\,s^{-1}$ between 0.3 and $1.5\,L\,s^{-1}$ and increased to $980.4\times10^{-4}\,J\,s^{-1}$ at $1.85\,L\,s^{-1}$ (Table 7). Froude efficiency, estimated as the ratio of thrust power output (total power minus energy lost to the wake) to total power output, ranged from 0.64 to 0.81 between 0.3 and $1.5\,L\,s^{-1}$ and decreased to 0.69 at $1.85\,L\,s^{-1}$.

Discussion

Undulatory locomotion in sirenid salamanders

Sirenid salamanders, like other undulatory swimmers, swim by propagating undulatory waves posteriorly along their body. These animals swim using an anguilliform mode, with an average of 1.5 propulsive waves along the length of their body at all speeds. These waves always move backwards faster than the animal is swimming forwards.

The amplitude of these undulatory waves typically increases along the entire body of the salamander. However, at higher speeds, the point of smallest undulatory amplitude is just posterior to the skull, as is typical of subcarangiform and carangiform swimmers (Webb, 1975). Videler (1981) suggested that undulatory amplitude increased linearly in an

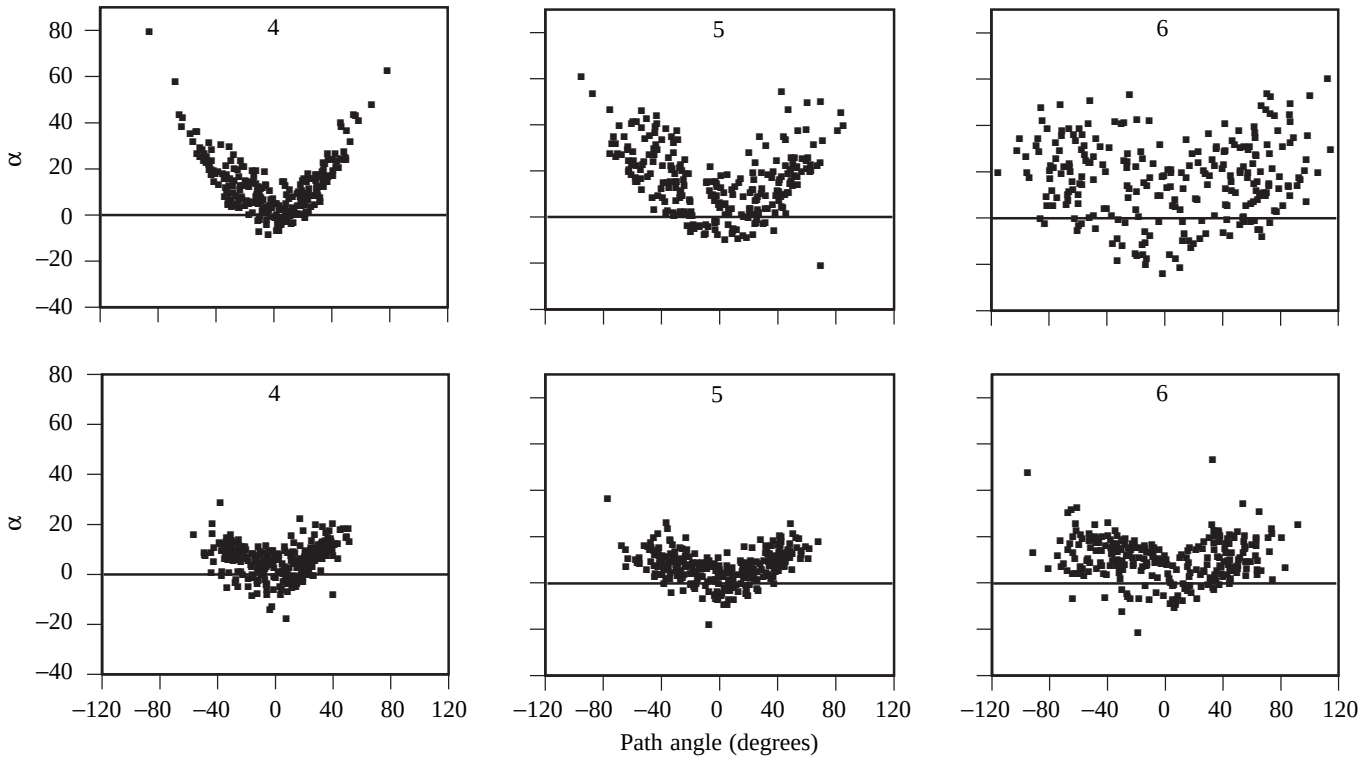

Fig. 11. Plots showing how the angle of attack of three tail segments (segments 4, 5 and 6 from left to right in each row; see Fig. 1G) varies as a function of where the segments are in an undulatory cycle for a slow ($0.3\,L\,s^{-1}$, upper panels) and a fast ($1.5\,L\,s^{-1}$, lower panels) swimming speed. During an undulatory cycle, a segment's path angle approaches zero as it becomes maximally laterally displaced to either side and approaches its highest absolute values (positive and negative values represent displacement to the right and left, respectively) as it nears the axis of forward progression (see Fig. 8). Segments tend to have negative angles of attack at low path angles (near maximum lateral displacement) and the highest angles of attack at high path angles (when passing the axis of forward progression). Note that, at the low swimming speed (top three panels), high angles of attack (greater than 20 °) are more prevalent than at the higher swimming speed.

Table 7. *Kinematic parameters used to estimate power output of swimming salamanders across a range of speeds*

U ($cm\,s^{-1}$)	V ($cm\,s^{-1}$)	f (s^{-1})	$2A_T$ (cm)	W ($cm\,s^{-1}$)	w ($cm\,s^{-1}$)	m_T ($g\,cm^{-1}$)	θ (degrees)	$10^{-4}\times E_T$ ($J\,s^{-1}$)	$10^{-4}\times E_K$ ($J\,s^{-1}$)	$10^{-4}\times E$ ($J\,s^{-1}$)
10.68	24.65	1.03	8.25	18.88	10.7	2.27	38.58	4.90	1.78	3.12
16.02	34.04	1.33	8.50	25.11	13.29	2.27	43.21	12.14	4.40	7.74
21.36	39.03	1.71	7.09	26.93	12.19	2.27	33.85	15.92	4.32	11.60
32.04	49.89	2.23	8.04	39.83	14.25	2.27	31.49	41.28	8.64	32.64
53.40	81.60	2.82	7.78	48.74	16.84	2.27	26.24	99.50	19.08	80.41
70.49	131.74	4.38	10.56	102.72	47.76	2.84	42.06	980.39	307.71	672.68

Calculations were performed according to Lighthill (1975) and Webb (1975).

Note that data from first five rows are taken from a 34 cm salamander, while data for last row (high-speed data) are taken from a 38.1 cm salamander.

Equations and symbols are taken from Webb (1975) and defined below.

U, swimming speed; V, traveling wave speed; f, tailbeat frequency; A_T, tailtip amplitude measured as defined in the text (A_T is multiplied by 2 in order to meet the definition of amplitude used in Lighthill, 1975); W, average lateral velocity of tailtip, $\pi(2A_T)f/2^{0.5}$; w, velocity of water being pushed by the tail, $W[(V-U)/V]$; m_T, virtual mass of the tail due to its acceleration of water, $\pi\rho d^2/4$, where ρ=1 (density of water) and d is the average tail depth; θ, average orientation of distal tail segment with respect to direction of forward travel; E_T, total power generated by salamander, $m_T wUW$; E_K, rate of kinetic energy lost to the wake, $0.5(m_T w^2 U)\cos\theta^{-1}$; E, thrust power, E_T-E_K.

anguilliform swimming eel (*Anguilla anguilla*). In *S. intermedia*, however, amplitude increases nonlinearly along the body at all speeds. Increases in amplitude per unit longitudinal distance along the body are relatively larger over the posterior portion of the trunk and the entire tail than over the anterior and middle portions of the trunk. Interestingly, while it is common for tail-tip amplitude to increase with swimming speed below speeds of $1–2\,L\,s^{-1}$ in a variety of

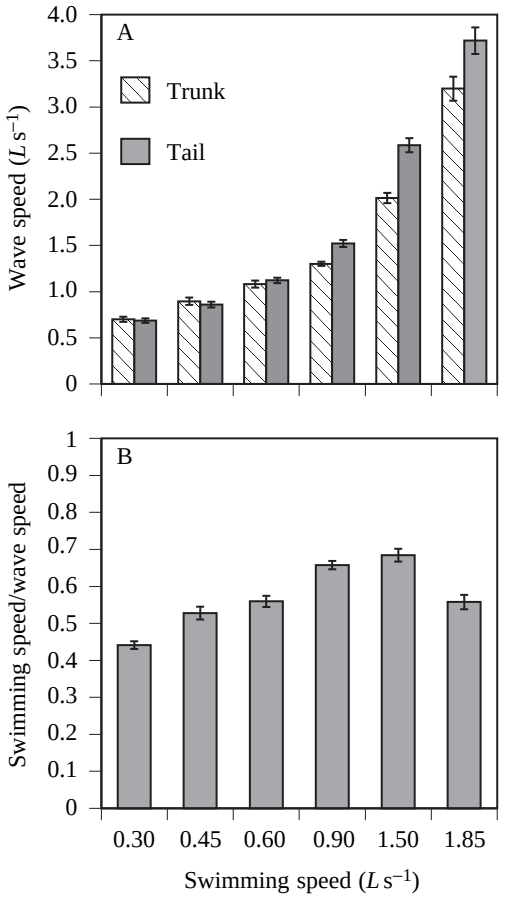

Fig. 12. (A) Traveling wave speed increases with swimming speed and changes along the body (it is higher along the tail than along the trunk) at higher swimming speeds. (B) If traveling wave speed is averaged along the whole body, the ratio of swimming speed to average wave speed (slip) increases with swimming speed except at the transition between 1.5 and 1.85 L s^{-1} where it decreases. Values are means ± S.E.M.

undulatory swimmers, this is not true of *S. intermedia*, where speed had no obvious effect on tail-tip amplitude between 0.3 and 1.5 L s^{-1} (Fig. 6A).

Flexion between intervertebral joints allows undulating swimmers to bend their bodies into a series of propulsive waves. Flexion was typically greatest at the joint between the base of the skull and the first vertebra. Despite high-amplitude undulatory displacements near the tip of the tail, intervertebral flexion in this region was relatively low because of the proportionate increase in the number of vertebrae per unit body length in this part of the axial skeleton.

As was pointed out by Jayne and Lauder (1993, 1995), in steadily swimming largemouth bass *Micropterus salmoides* and during fast-starts in bluegill sunfish *Lepomis gibbosus*, maximum lateral displacement and maximal flexion of a given point along an undulator's body do not coincide in time. The same is true for sirenid salamanders, where maximal flexion usually occurs prior to maximal lateral displacement. Therefore, using points of maximum lateral displacement to define points of maximum curvature along the body is unwarranted in this species and this might be true of other anguilliform swimmers as well.

The path of travel of points along the salamander's body typically follows a sinusoidal pattern. Occasionally, however, a unique kinematic pattern is observed. At the slowest speeds (0.3 and 0.45 L s^{-1}) and the fastest speed (1.85 L s^{-1}), the maximum path angle of points near the tip of the tail can actually be equal to or slightly greater than 90 ° relative to the axis of forward progression. As these points sweep laterally from side to side during a tail beat, they can at times be moving perpendicular or even slightly backwards (obtuse path angle) relative to the direction of locomotion, while the animal is swimming forwards. Hence, as the salamander is swimming, distal portions of the tail can be moving backwards faster than the animal is moving forwards.

Close examination of salamander tail kinematics reveals that there are consistent periods during which segments along the tail have negative angles of attack (Fig. 10A). Negative angles of attack of the tail have also been found in a variety of swimming fishes, including largemouth bass *Micropterus salmoides* (Jayne and Lauder, 1995), goldfish *Carassius auratus* and dace *Leuciscus leuciscus* (Bainbridge, 1963). However, there are animals that swim *via* undulatory movements of the tail and maintain positive angles of attack at the tail during the entire undulatory cycle, such as tuna *Euthynnus affinis* (Fierstine and Walters, 1968) and bottlenose dolphin *Tursiops truncatus* (Fish, 1993). Increased stiffness within the tail region due to morphological specialization within these animals may be responsible for the continued maintenance of a positive angle of attack throughout the undulatory cycle (Jayne and Lauder, 1995). Sirenid salamanders have tails that are extremely flexible, with many small vertebrae, and so it is indeed possible that increased mechanical flexibility within the tail region is a factor that leads to negative angles of attack when segments are near their maximum lateral displacement. Positive angles of attack of tail segments tended to be greatest at low swimming speeds, and this trend is also seen in other animals, such as bass and dolphin, where the effects of speed have been examined (although bass showed high maximum positive values of angle of attack at the lowest and highest swimming speed, with lower intermediate values; Jayne and Lauder, 1995).

Effects of speed on kinematics

Although swimming speed did not have a statistically significant effect upon many kinematic variables, including the amplitude of lateral displacement, intervertebral flexion, path angle and orientation of body segments (θ), this does not necessarily imply that speed has no real effect on these variables. For example, one potential reason for the lack of a statistical speed effect (between 0.3 and 1.5 L s^{-1}) is that sample size was low (N=4). A small sample size makes finding subtle and complex differences due to fixed statistical effects more difficult owing to the reduced degrees of freedom in the denominator mean squares. An examination of the data

suggests that speed might have consistent, but subtle, effects on displacement (there were consistent increases with speed from the middle of the trunk to near the middle of the tail; Fig. 6A), flexion (which increases with speed in the anterior portions of the trunk and decreases with speed in the posterior part of the tail; Fig. 6B), path angle (which decreases with speed along the tail; Figs 6C, 8B) and orientation (which decreases with speed at the tip of the tail; Fig. 8C), despite the lack of statistical significance.

Another potential reason why speed did not show a statistically significant effect on these kinematic variables is that one individual tended to swim with relatively high-amplitude excursions anteriorly at slow swimming speeds. The undulatory amplitude, intervertebral flexion, path angles and segment orientation of this individual were therefore much greater along the head and front half of the trunk at slow speeds than for the other three individuals (hence the significant speed × individual and site × individual statistical interactions for most of these kinematic variables). Therefore, this individual's pattern of movement at slow speed (particularly over the front half of its body) was more similar to the other individuals' patterns of movements at higher speeds, making it difficult (particularly given the small sample size) to find a significant effect of swimming speed on these variables.

An additional reason to suspect that speed can have effects on these kinematic parameters is that kinematic patterns from the single sequence at $1.85\,L\,s^{-1}$ are distinct from patterns at all other swimming speeds. *S. intermedia* are relatively sedentary and spend much of their time concealed in vegetation or burrows (Mount, 1975), and it is probable that very high-speed swimming is rarely used and might involve unique or exaggerated muscle activity patterns relative to slower swimming, explaining these distinct kinematic patterns.

Power output and efficiency during swimming

As direct measurements of the energy used for propulsion and lost to the surrounding fluid during swimming are technically difficult, hydrodynamic models which relate kinematic parameters to power output are often used to measure the thrust production of undulatory swimmers indirectly. One group of hydrodynamic models considers the 'resistive' forces acting on body and tail segments due to their respective angles of attack and velocities (e.g. Taylor, 1952). Such 'quasi-static' analyses are appropriate for animals swimming at low Reynolds numbers (Re<1000), or animals with 'bad hydromechanical shape' (animals approximately circular in cross section, rather than being laterally compressed and relatively deep-bodied) swimming at higher Reynolds numbers (Lighthill, 1975; Webb, 1975). Another group of hydrodynamic models considers the 'reactive' forces acting on an animal due to the acceleration of a 'virtual mass' of water along the length of the body as a result of the animal's undulatory movements. The momentum of this mass of water is finally shed at the trailing edge of the tail, providing forward thrust to the animal (e.g. Lighthill, 1975).

It is generally agreed that anguilliform swimmers utilize both resistive and reactive forces during swimming (Lighthill, 1975; Webb, 1975), but that models considering reactive forces are better for determining power output and efficiency during swimming (Webb, 1975). Therefore, following Lighthill's reactive bulk-momentum model (1975), total power output, thrust power (which does not include energy lost to the wake) and Froude efficiency were calculated for one individual at each swimming speed (Table 7).

Total power output, energy lost to the wake and useful power output all increase with swimming speed. Froude efficiency of swimming *S. intermedia* (measured as thrust power divided by total power) also increases with swimming speed from 0.64 at $0.3\,L\,s^{-1}$ to 0.81 at $1.5\,L\,s^{-1}$ but then decreases at the high-speed trial of $1.85\,L\,s^{-1}$ (using data for one individual) to an intermediate value of 0.69. Froude efficiency can also be estimated as $1–0.5[(V–U)/V]$, or $(U+V)/2V$ (Webb, 1975), where U is the swimming velocity and V is the velocity of the traveling wave. Using this equation results in slightly different values, but the values follow a similar trend, increasing from 0.72 at $0.3\,L\,s^{-1}$ to 0.83 at $1.5\,L\,s^{-1}$ and again decreasing at $1.85\,L\,s^{-1}$ to 0.77, suggesting that swimming efficiency is lowest at low swimming speeds, but might also decrease at very high swimming speeds.

It has been shown in several aquatic vertebrates that propulsive efficiency is typically low at slow swimming speeds and increases asymptotically to a maximum value with increasing swimming speed [e.g. trout (Webb *et al.* 1984), tadpoles (Wassersug and von Seckendorf Hoff, 1985) and ambystomatid salamander larvae (von Seckendorf Hoff *et al.* 1989), although see Frolich and Biewener (1992) for different results]. Interestingly, *S. intermedia* also show an increase in Froude efficiency with swimming speed up to $1.5\,L\,s^{-1}$. However, rather than reaching an asymptote at higher speeds, a swimming trial at $1.85\,L\,s^{-1}$ showed a decreased Froude efficiency. Low efficiencies at the lowest and highest speeds can be partially explained by the relatively large average angle (θ) between the distal portion of the tail and the direction of forward travel at these speeds (Table 7). In the reactive model used to calculate power output and Froude efficiency, θ plays an important role in determining the amount of the total energy that is lost to the wake. Energy lost to the wake increases by a factor of $1/\cos\theta$; hence, greater average values of θ necessitate a larger amount of energy lost to the wake and, accordingly, lower Froude efficiencies.

In addition, Lighthill (1977) suggested that a substantial amount of energy can be lost into the wake as a result of lateral recoil movements in the anterior region of the body of a carangiform swimmer. While Lighthill's model for quantifying relative energy loss due to anterior recoil did not apply to anguilliform swimming, it is certainly possible that the exaggerated yaw at the tip of the snout during swimming at $1.85\,L\,s^{-1}$ may also account, in part, for the decreased Froude efficiency at this speed.

Taxonomic comparisons of anguilliform locomotion

Both external and internal morphological features vary

Table 8. *Comparative kinematic data for a variety of similarly sized anguilliform swimming vertebrates: freshwater eel (*Anguilla *sp.), fully aquatic salamander (*Siren intermedia*), nonconstricting colubrid snake (*Nerodia fasciata pictiventris*), constricting colubrid snake (*Elaphe g. guttata*) and a sea snake (*Pelamis platurus*)*

Variable	*Anguilla*[1] (35–40 cm)	*Siren*[2] (34–38 cm)	*Nerodia*[3] (22–39 cm)	*Elaphe*[3] (33–41 cm)	*Pelamis*[4] (51 cm)
Slope of relationship between length-specific swimming speed (y) and tailbeat frequency (x)	0.5	0.51	0.46	0.38	0.38
Length-specific tailbeat amplitude relative to the axis of forward progression	0.07–0.09	0.11–0.14	0.12–0.19	0.12–0.14	0.12–0.13
Speed of mechanical wave	Remains constant	Increases along body at high speeds	Increases along body[5]	Increases along body[5]	Increases along body[5]

[1]Personal observation or Grillner and Kashin (1976).
[2]This study.
[3]Jayne (1985).
[4]Graham *et al.* (1987).
[5]Studies reported that half-wavelengths increased along the body.
Total lengths are given in parentheses.

considerably across anguilliform-swimming elongate vertebrates that have been studied to date. Eels (*Anguilla* sp.) are somewhat laterally compressed over much of their length and have increased depth due to dorsal and ventral fins which span most of their body. Swimming salamanders and many swimming snakes, in contrast, are typically circular in cross section and have tails of varying length that may or may not be laterally flattened. Numbers of vertebrae can vary dramatically, from over 250 in certain snake species to less than 100 in some salamanders. However, despite such morphological differences, kinematic similarities have often been emphasized across different anguilliform taxa, and such similarities are often explained, in part, as being the result of hydrodynamic constraints acting on an elongate body undulating through water (Jayne, 1985). However, closer inspection of data from a variety of anguilliform swimmers suggests that substantial kinematic variation exists within this swimming mode.

It is well known that the swimming speed of an undulating fish is related to its tailbeat frequency and amplitude (Bainbridge, 1958). Swimming speed typically increases linearly with tailbeat frequency in anguilliform taxa. However, the quantitative nature of this relationship varies across these taxa. Swimming speed increases fastest with tailbeat frequency in *S. intermedia* (this study) and eels (*Anguilla* sp.; Grillner and Kashin, 1976) and slowest in rat snakes (*Elaphe g. guttata*; Jayne, 1985) and sea snakes (*Pelamis platurus*; Graham *et al.* 1987) (Table 8). Tailbeat amplitude also affects swimming speed, and an examination of amplitudes across these taxa also shows some variation; values are consistently lower in swimming eels (Grillner and Kashin, 1976; G. B. Gillis, personal observation) than in other taxa and are particularly high in water snakes (*Nerodia fasciata pictiventris*; Jayne, 1985) (Table 8).

At least some of this kinematic variability across taxa is correlated with external morphological differences. Eels are laterally compressed along much of their body and maintain their body depth with long, continuous dorsal and ventral fins. As Lighthill (1975) noted, lateral compression of the posterior portion of an anguilliform swimmer's body tends to improve swimming speed and hydromechanical efficiency greatly. The lateral motion of a deep, laterally compressed tail facilitates a relatively greater transfer of momentum from the animal to the water because it produces a significant virtual mass of water relative to a tapering tail that is not laterally compressed (Lighthill, 1975).

Comparative data support this notion, as eels increase swimming speed rapidly with tailbeat frequency and use a relatively low tailbeat amplitude in doing so. It is likely that the external morphological features of eels (especially the long, deep, laterally compressed tail) play a large role in allowing them to do this. *S. intermedia*, although nearly round in cross section along their trunk, like snakes, also increase swimming speed with tailbeat frequency faster relative to the snakes studied to date, despite using similar or lower undulatory amplitudes to do so. However, these salamanders also have laterally compressed tails along the posterior 30% of their body, whereas the tails of most snakes are not laterally compressed and taper to a point (although not in *Pelamis platurus*). Possession of a relatively long laterally compressed tail probably facilitates relatively rapid increases in swimming speed with increases in tailbeat frequency in *S. intermedia*.

Snake species studied to date tend to increase swimming speed relatively slowly with increases in tailbeat frequency and/or use relatively higher amplitudes at the tip of the tail (Table 8). This is even true of sea snakes (*Pelamis platurus*), despite their laterally compressed bodies. One possible reason is that many generalized snakes are buoyant and tend to swim at or near the water surface when using anguilliform locomotion. Jayne (1988) showed that there were significant differences between muscle activity patterns used when an

individual water snake (*Nerodia fasciata*) was swimming at the water surface relative to when it was swimming fully submerged. Hence, it is possible that differences in muscle activity patterns across taxa and/or differences in locomotor resistance due to wave formation or other interactions with the surface create the kinematic differences seen between surface-swimming snakes and the eels and salamanders that swim well below the surface of the water.

It is also possible that internal morphological differences, such as differences in vertebral numbers, might also lead to taxonomic differences in undulatory movement patterns. Jayne's work on swimming snakes (1985, 1988) with radically different numbers of vertebrae suggests that kinematic patterns are not obviously affected by differences in the number of axial skeletal elements along the body. Additionally, in the present study, one individual salamander had 23% fewer vertebrae than the other three salamanders (Fig. 5). However, in *post-hoc* tests, this individual did not stand out as having significantly different kinematic patterns relative to those of the other three individuals. Therefore, it appears that differences in the numbers of vertebrae among or within the anguilliform taxa studied to date do not have drastic effects upon the patterns of movements used by these animals during swimming.

To understand better if and how the evolution of an elongate body affects undulatory locomotor behavior, we need more quantitative kinematic and electromyographic data from anguilliform swimming taxa. These data would then provide more insight into the extent and nature of variability within this phylogenetically diverse locomotor mode. Once an understanding of this variability is available, quantitative comparisons between anguilliform and subcarangiform or carangiform modes of locomotion will be possible and should help us define better and understand locomotor differences between the morphologically divergent animals that utilize these traditional categories of undulatory locomotion.

I would particularly like to thank both Larry Raymond and Beth Brainerd for their help in providing me with salamanders. George Lauder, Al Bennett and Tim Bradley have given me useful comments and advice during all phases of this project. In addition, this manuscript has been improved significantly by comments from George Lauder, Al Bennett, Miriam Ashley-Ross, Alice Gibb, Lara Ferry, Amy Cook, Jim O'Reilly and two anonymous reviewers. Finally, without the reliable assistance of Peter Rim and Michael Erickson, I would still be digitizing video fields of swimming salamanders. The high-speed video was obtained under NSF grant BBS 8820664 and this research was supported by NSF grant IBN 95-07181 to George Lauder.

References

ARCHER, S. D. AND JOHNSTON, I. A. (1989). Kinematics of labriform and subcarangiform swimming in the antarctic fish *Notothenia neglecta*. *J. exp. Biol.* **143**, 195–210.

AUFFENBERG, W. (1962). A review of the trunk musculature in the limbless land vertebrates. *Am. Zool.* **2**, 183–190.

BAINBRIDGE, R. (1958). The speed of swimming of fish as related to size and to the frequency and amplitude of the tail beat. *J. exp. Biol.* **35**, 109–133.

BAINBRIDGE, R. (1963). Caudal fin and body movement in the propulsion of some fish. *J. exp. Biol.* **40**, 23–56.

BREDER, C. M. (1926). The locomotion of fishes. *Zoologica* **4**, 159–297.

FIERSTINE, H. L. AND WALTERS, V. (1968). Studies in locomotion and anatomy of scombroid fishes. *Mem. S. Calif. Acad. Sci.* **6**, 1–31.

FISH, F. E. (1993). Power output and propulsive efficiency of swimming bottlenose dolphins (*Tursiops truncatus*). *J. exp. Biol.* **185**, 179–193.

FROLICH, L. M. AND BIEWENER, A. A. (1992). Kinematic and electromyographic analysis of the functional role of the body axis during terrestrial and aquatic locomotion in the salamander *Ambystoma tigrinum*. *J. exp. Biol.* **162**, 107–130.

GANS, C. (1975). Tetrapod limblessness: evolution and functional corollaries. *Am. Zool.* **15**, 455–467.

GRAHAM, J. B., LOWELL, W. R., RUBINOFF, I. AND MOTTA, J. (1987). Surface and subsurface swimming of the sea snake *Pelamis platurus*. *J. exp. Biol.* **127**, 27–44.

GRAY, J. (1933). Studies in animal locomotion. I. The movement of fish with special reference to the eel. *J. exp. Biol.* **10**, 88–104.

GRILLNER, S. AND KASHIN, S. (1976). On the generation and performance of swimming in fish. In *Neural Control of Locomotion* (ed. R. M. Herman, S. Grillner, P. S. Stein and D. G. Stuart), pp. 181–201. New York: Plenum Press.

JAYNE, B. C. (1985). Swimming in constricting (*Elaphe g. guttata*) and nonconstricting (*Nerodia fasciata pictiventris*) colubrid snakes. *Copeia* **1985**, 195–208.

JAYNE, B. C. (1988). Muscular mechanisms of snake locomotion: An electromyographic study of lateral undulation of the Florida banded water snake (*Nerodia fasciata*) and the yellow rat snake (*Elaphe obsoleta*). *J. Morph.* **197**, 159–181.

JAYNE, B. C. AND LAUDER, G. V. (1993). Red and white muscle activity and kinematics of the escape response of the bluegill sunfish during swimming. *J. comp. Physiol.* A **173**, 495–508.

JAYNE, B. C. AND LAUDER, G. V. (1995). Speed effects on midline kinematics during steady undulatory swimming of largemouth bass, *Micropterus salmoides*. *J. exp. Biol.* **198**, 585–602.

LIGHTHILL, J. (1975). *Mathematical Biofluiddynamics.* Bristol: J. W. Arrowsmith Ltd.

LIGHTHILL, J. (1977). Mathematical theories of fish swimming. In *Fisheries Mathematics* (ed. J. H. Steele), pp. 131–144. New York: Academic Press.

LONG, J. H., MCHENRY, M. J. AND BOETTICHER, N. C. (1994). Undulatory swimming: how traveling waves are produced and modulated in sunfish (*Lepomis gibbosus*). *J. exp. Biol.* **192**, 129–145.

MOUNT, R. H. (1975). *The Reptiles and Amphibians of Alabama* Auburn: Auburn Printing Co.

RICE, W. R. (1989). Analyzing tables of statistical tests. *Evolution* **43**, 223–225.

SOKAL, R. R. AND ROHLF, F. J. (1981). *Biometry* (2nd edn). New York: W. H. Freeman and Co.

TAYLOR, G. (1952). Analysis of the swimming of long narrow animals. *Proc. R. Soc. Lond.* A **214**, 158–183.

VIDELER, J. J. (1981). Swimming movements, body structure and propulsion in cod *Gadus morhua*. *Symp. zool. Soc. Lond.* **48**, 1–27.

VIDELER, J. J. AND HESS, F. (1984). Fast continuous swimming of two pelagic predators, saithe (*Pollachius virens*) and mackerel (*Scomber scombrus*): a kinematic analysis. *J. exp. Biol.* **109**, 209–228.

VOGEL, S. (1983). *Life in Moving Fluids.* Princeton: Princeton University Press.

VON SECKENDORF HOFF, K., HUQ, N., KING, V. A. AND WASSERSUG, R. J. (1989). The kinematics of larval salamander swimming (Ambystomatidae: Caudata). *Can. J. Zool.* **67**, 2756–2761.

WASSERSUG, R. J. AND VON SECKENDORF HOFF, K. (1985). The kinematics of swimming in anuran larvae. *J. exp. Biol.* **119**, 1–30.

WEBB, P. W. (1975). Hydrodynamics and energetics of fish propulsion. *Bull. Fish. Res. Bd Can.* **190**, 1–158.

WEBB, P. W. (1993). The effect of solid and porous channel walls on steady swimming of steelhead trout *Oncorhynchus mykiss*. *J. exp. Biol.* **178**, 97–108.

WEBB, P. W. AND BLAKE, R. W. (1985). Swimming. In *Functional Vertebrate Morphology* (ed. M. Hildebrand, D. M. Bramble, K. F. Liem and D. B. Wake), pp. 110–128. Cambridge: Belknap Press.

WEBB, P. W., KOSTECKI, P. T. AND STEVENS, D. E. (1984). The effect of size and swimming speed on locomotor kinematics of rainbow trout. *J. exp. Biol.* **109**, 77–95.

ZAR, J. H. (1984). *Biostatistical Analysis* (2nd edn). Englewood Cliffs: Prentice-Hall, Inc.